

High-pressure microfluidic systems (HPMS): flow and cavitation measurements in supported silicon microsystems

Thomas Gothsch · Christiane Schilcher ·
Claudia Richter · Stefan Beinert · Andreas Dietzel ·
Stephanus Büttgenbach · Arno Kwade

Received: 8 October 2013 / Accepted: 6 May 2014 / Published online: 22 May 2014
© Springer-Verlag Berlin Heidelberg 2014

Abstract Conventionally fabricated silicon microfluidic systems with glass coverage were stabilized by a specially developed frame to withstand high-pressure drops of up to 500 bar. Velocity measurements were carried out with an optical non-intrusive measurement technique (μ PIV) to characterize the flow in the microfluidic systems. High-pressure applications in microsystems differ compared to more conventional microfluidic applications especially in the higher Reynolds numbers up to 11,500, higher shear forces and the presence of hydrodynamic cavitation. In order to characterize the cavitation phenomena, a photo-optical cavitation measurement technique on the basis of a μ PIV setup was applied to visualize the cavitation pattern. The flow of a T- and an orifice geometry were investigated. It was found out that hydrodynamic cavitation, which is a source of abrasion, influences the flow to a great extent

and, in orifice geometries, also the volume flow. By applying a backpressure cavitation could be decreased and, at a sufficiently high backpressure, eliminated. Besides the photo-optical cavitation measurements, volume flow measurements could be used to determine the critical backpressure at which cavitation is restricted to the vena contracta in orifice microchannels. With the presented techniques, beginning with the micro fabrication process over the external stabilization up to the high-speed flow characterization, a concept of a high-pressure microfluidic system is introduced, which is suitable for a wide range of applications in research and process development in high-pressure microsystems.

Keywords High pressure · Cavitation · Orifice · Turbulence · μ PIV · Silicon microsystem · HPMS

T. Gothsch (✉) · C. Schilcher · S. Beinert · A. Kwade
Institute for Particle Technology, TU Braunschweig,
Volkmaroderstr. 5, 38104 Brunswick, Germany
e-mail: t.gothsch@tu-bs.de

C. Schilcher
e-mail: c.schilcher@tu-bs.de

S. Beinert
e-mail: s.beinert@tu-bs.de

A. Kwade
e-mail: a.kwade@tu-bs.de

C. Richter · A. Dietzel · S. Büttgenbach
Institute of Microtechnology, TU Braunschweig,
Alte Salzdahlumer Str. 203, 38124 Brunswick, Germany
e-mail: claudia.richter@tu-bs.de

A. Dietzel
e-mail: a.dietzel@tu-bs.de

S. Büttgenbach
e-mail: s.buettgenbach@tu-bs.de

1 Introduction

Process engineering using microsystems features a couple of advantages compared to standard process engineering like higher energy and substance efficiency due to minimized heat and mass transport resistances and higher process speeds. Additionally, it usually enables a more rapid and cost-efficient process development due to standardized and fast fabrication processes, reduced investment costs and little reactant volumes. In particular, the latter advantage recommends small-scale devices for screening applications. The conventionally utilized substrates for the fabrication of fluidic microsystems are glass, silicon and polymers like polydimethylsiloxane (PDMS) (Capretto et al. 2013). Independent of the substrate, all these types of microsystems exhibit the opportunity of an optical observation, which is an important requirement in scientific

research and for process development. The disadvantage of these kinds of microsystems is the low rigidity of the substrates which limits the maximum pressure drop within the microsystems practically to about 20 bar (Mishra and Peles 2005; Li et al. 2005; Gravesen et al. 1993). This limitation does not pertain for metal-based microsystems due to their high rigidity (Richter et al. 2013). But the high rigidity is accompanied by the loss of an optical access which, as mentioned above, is a crucial disadvantage for applications in research and process development. Nevertheless, all these fabrication processes facilitate complex and accurate microstructures and, thus, enable the arrangement of a whole process chain on one microsystem. Pressure difference is the driving force for the fluid movement in microsystems and is usually applied from the outside. Microchannels inherently exhibit very high-pressure losses due to the diminutive scale. In consequence, the limitation in maximum pressure is accompanied by further confinements like limited flow velocities which result in low Reynolds numbers and, hence, in laminar flow. These limitations have consequences for several unit operations in process engineering like mixing. Turbulent mixing does not occur in conventional microfluidic systems, and hence, mixing processes base on diffusive mixing which is an inherently slow process (Lee et al. 2011). Therefore, passive or active micromixers have to be implemented which usually increase the complexity of the microsystems, claim space and, nevertheless, are limited in mixing rate and throughput. However, precipitation processes with high reaction rates, for example, are dependent on high mixing rates and a thorough mixing performance. The limitations can be solved by enabling turbulent flow in microfluidic systems by realizing higher pressure differences. With sufficiently high fluid velocities, high shear forces can be generated, which enable new processes such as dispersion or emulsification processes in fluidic microsystems (Gothsch et al. 2011; Beinert et al. 2012). The aim of this work was to develop a high-pressure microfluidic system (HPMS) for research applications and process development which enables non-intrusive flow characterization and is based on an established microfabrication process.

In HPMS, problems like deposits or undesirable gas bubbles decrease in their importance due to the high velocities and the turbulent flow regime but other phenomena like hydrodynamic cavitation or high shear forces arise and have to be characterized and subsequently controlled. In particular, cavitation poses challenges due to the fact that it can enormously influence the flow, shear forces and surely mixing performance. Additionally, it can be the source of abrasion in microsystems. High shear forces can, on the one hand, enable dispersion or emulsification processes but, on the other hand, lead to damage of sensitive products. In contrast to the laminar flow in low-pressure microsystems,

the prediction of the flow in HPMS by means of CFD simulations is much more complex and less accurate. Main reasons are the simultaneous presence of laminar and turbulent flow and the cavitating (two-phase) flow. Thus, characterization of the flow and the hydrodynamic cavitation in HPMS is an essential requirement in process development and microchannel design. After the development of a process in the presented silicon-based microsystems, the working and characterized microchannel geometry can be transferred to metal-based microsystems for industrial usage. However, HPMS in general (silicon-based or metal-based) exhibit some disadvantages which have to be taken into account. Compared to conventional low-pressure processes, high-pressure processes exhibit much higher energy consumption and higher costs for peripheral equipment.

High pressure, high fluid velocities and channel dimensions in the micrometer range pose extraordinary challenges to the flow characterization system and are the reason for the absence of high-resolution flow measurements in this field so far. Flow characterizations in high-pressure microstructures were conducted especially in the field of high-pressure emulsification and in the diesel engine injection technology. Early flow measurements in microstructures were conducted with sensors which were implemented directly into the flow or in holes in the wall (Phipps 1974). These intrusive measurements always affect the flow or the pressure in an unknown manner, and in consequence, the accuracy of the results is also unknown. Additionally, the local resolution of the measurements is relatively low. In consequence, visual techniques were utilized to earn more information of the flow in high-pressure microchannels without affecting it. Phipps (1974) carried out photographic and visual investigations without a magnification concerning the extent of cavitation and flow separation in a homogenizing poppet valve. Mishra and Peles (2005) utilized silicon microsystems, very similar to those used in this paper, to carry out cavitation measurements but due to the inherently low stability of the microsystems, they were restricted to a maximum pressure of 13.1 bar. In order to enable cavitation at low fluid velocities anyway, they reduced the pressure at the outlet of the microsystem below the atmosphere pressure which led to crucial differences in the cavitation behavior and especially in the collapse behavior, compared to high velocity flows with ambient pressure at the outlet like in this paper. Håkansson et al. (2010) utilized a microscope with a $5\times$ objective and a laser as a high-intensity light source to visualize cavitation in a high-pressure cell up to a maximum pressure of 120 bar. Additionally, numerous cavitation measurements concerning diesel nozzles were carried out mainly with scale-ups and at moderate pressures (Sou et al. 2007; Suh and Lee 2008; Salvador et al. 2013). Beside photo-optical cavitation measurements, “microparticle image velocimetry” (μ PIV)

enables flow measurements with high resolution in microchannels and also in turbulent flow, as for example Li showed with low-pressure experiments in PDMS systems (Li and Olsen 2006a, b; Li et al. 2005).

In this paper, techniques for the fabrication and characterization of HPMS with an optical access, on basis of the established fabrication process of silicon microsystems, are presented. Conventional low-pressure silicon microsystems with glass coverage were stabilized by a specially developed construction to withstand high-pressure drops of up to 500 bar. Flow measurements with an optical non-intrusive measurement technique (μ PIV) were carried out to characterize the flow in the HPMS. In order to characterize the cavitation phenomena, a photo-optical cavitation measurement on basis of a μ PIV setup was applied to visualize the cavitation pattern. In the following, the flow of simple microchannel geometries originating from the disintegration of droplets and agglomerates is characterized. These simple geometries were chosen in order to achieve very high velocities and distinct regimes of hydrodynamic cavitation showing the potential of the measurement techniques and the differences to low-pressure microsystems.

2 Materials and methods

2.1 Microsystem

The utilized microsystems consist of a silicon plate including the microchannels at the top side and the inlet and outlet at the bottom side. The microstructures are fabricated by a double-sided, deep-reactive ion dry etching process (Lesche et al. 2011; Büttgenbach et al. 2009). The microchannel is covered by a Pyrex glass plate with a thickness of 500 μ m in an anodic bonding process. The glass plate enables an optical access to the microchannel from the top side (see Fig. 1a). Due to the fabrication process, all utilized microchannels exhibit a rectangular cross-sectional area (see Fig. 1b).

The silicon microsystem is fixed in a frame which counteracts the pressure inside the microchannel and, thus, enables high-pressure stability in the relatively fragile microsystems. Additionally, the frame enables a leak proof and reversible connection between the microsystem and the high-pressure equipment. In Fig. 2a an orifice microchannel with feed pipes (diameter: 1.5 mm), which are integrated in

Fig. 1 Schematic diagram of the silicon microsystem with inlet and outlet at the bottom side and a glass coverage at the top side (a); REM image of a silicon microchannel (b)

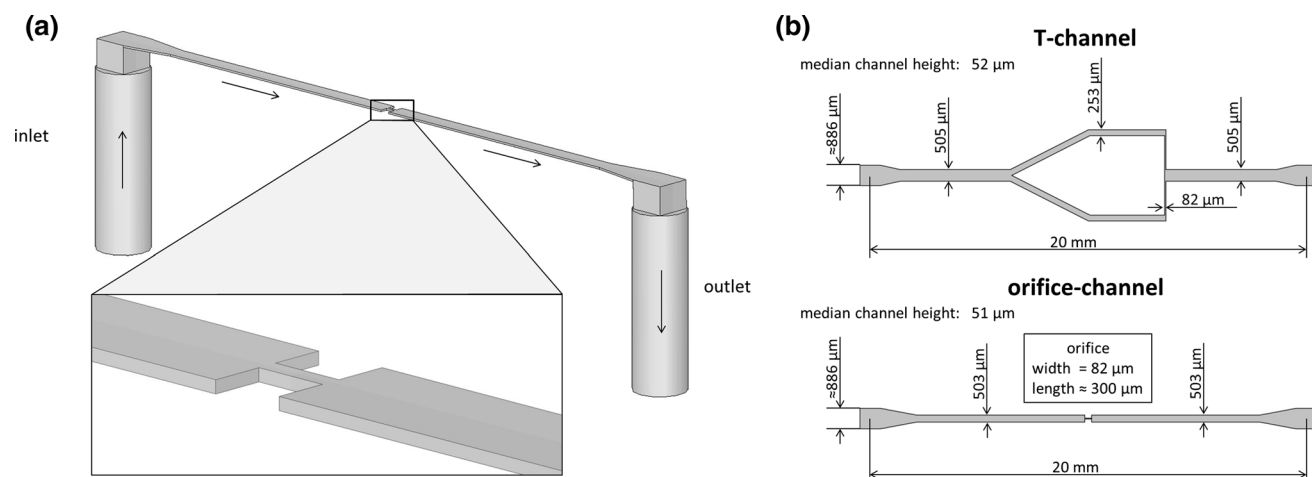
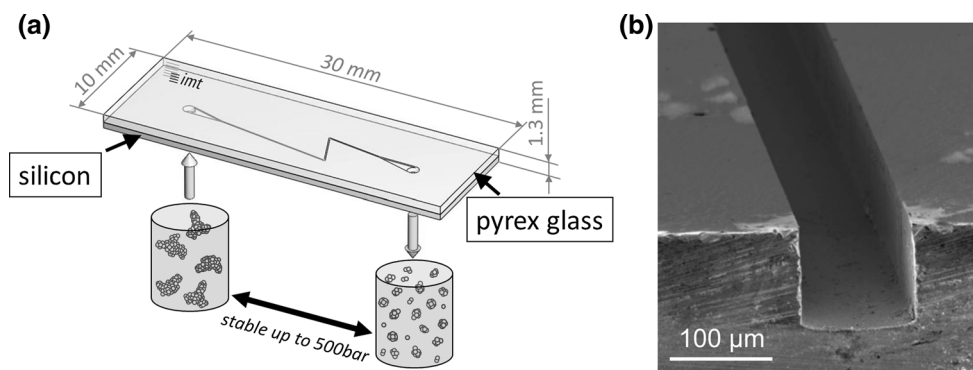


Fig. 2 Microchannel with feed pipes of the microsystem frame (a); dimensions of the investigated microchannel geometries (b)

the microsystem frame, is depicted. The dimensions of the investigated microchannel geometries (orifice and T-channel) were measured with the surface profiler Dektak 8 (Bruker) and are depicted in Fig. 2b. Dimensions marked with an approximately equals sign could not be measured. However, small deviations of the dimensions at the respective places do not affect the results in a noticeable degree.

2.2 High-pressure installation

Flow measurements were carried out with the high-pressure installation shown in Fig. 3. The pressure is generated by a pressure transducer (Dustec) which enables to pump 145 mL at pressures up to 4,000 bar without pulsation. The static pressure is measured with two manometers p_I and p_B (P2VA1, HBM, accuracy class: 0.2, $p_{\max} = 3,000$ bar) in front and behind the microsystem. Due to the fact that the pressure losses in the feed pipes between the manometers and the in-/outlet of the microsystem are far below 1 bar, they can be neglected. This was estimated by pumping a volume flow which was 5 times higher through the feed pipes. Even at this high volume flow, the pressure loss was below 1 bar. It follows that the pressure p_I is consistent with the pressure at the inlet and the pressure p_B (back-pressure) is consistent with the pressure at the outlet of the microsystem. By closing the regulating valve, a certain backpressure p_B at the outlet of the microsystem can be set. A backpressure of zero bar ($p_B = 0$) indicates ambient pressure. The microsystem is positioned upside down in the microsystem frame, and the flow measurements were carried out from the bottom side.

2.2.1 Microsystem frame

The silicon–glass microsystems with a thickness of about 1.3 mm are brittle and, without further measures, limited in pressure stability up to a few bar. In order to make them withstand pressures of up to 500 bar, a 5-mm-thick quartz glass plate is pressed on the glass side of the microsystem with a force of about 10 kN. On the silicon side, a flat,

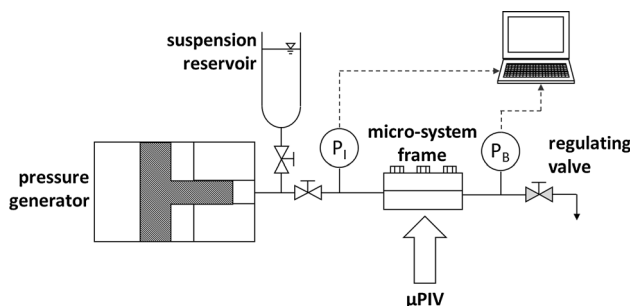


Fig. 3 High-pressure installation

polished steel surface is pressed. The surfaces have to be flat, rigid and parallel to the microsystem surface. The gap in the metal frame for the optical measurements is kept as small as possible to protect the quartz glass from breakage. The whole construction is a compromise between mechanical stability and quality of the optical access.

2.3 Flow measurements

For the flow measurements, a μ PIV system (LaVision GmbH) consisting of an inverted epifluorescent microscope (Axio Observer Z1, Zeiss), two 12 bit CCD cameras (Imager Intense, LaVision GmbH) with a resolution of $1,376 \times 1,040$ pixels and a Nd:YAG double pulse laser (Nano S, Litron) with a wave length of 532 nm were used. Monodisperse fluorescent particles on polystyrene basis in distilled water (PS-Fluo Red-1, microparticles GmbH) with a diameter of 1 μm were applied to seed and track the flow in the μ PIV measurements. Due to the high velocities, a single camera with a minimal interframing time of 500 ns was not sufficient. In order to further reduce the possible interframing time, two CCD cameras with a 50:50 beam splitter were applied. The first laser pulse was timed straight at the end of the exposure of the first camera, and the second laser pulse was timed straight at the beginning of the exposure of the second camera. The laser pulses had a length of 6 ns. Thus, a minimal interframing time of 100 ns could be enabled. The velocity vectors were calculated with the Software Davis 7 (LaVision GmbH). Due to the unsteady turbulent flow downstream of the orifice, only instantaneous velocity measurements are shown.

In order to visualize the vapor and liquid phase in the cavitation measurements, the fluorescent pigment Rhodamin B was dissolved in water and the channel was illuminated with the laser from the top. The reflected laser light was filtered out, and the fluorescent light was detected with the CCD cameras. Due to the different concentrations of the pigment in the vapor and liquid phase, it is possible to distinguish the phases in the images. Instantaneous cavitation images were recorded with a frequency of 9 Hz and an exposure time of 6 ns (laser pulse). The averaged images are averaged over 100 instantaneous images. A colored scale from blue, which represents a low fluorescent intensity, to white, which represents a high fluorescent intensity, was chosen to visualize the different phases.

In order to characterize the potential of a flow to cavitate, the cavitation number CN is used:

$$CN = \frac{p_I - p_B}{p_B - p_v}$$

where p_v is the vapor pressure of the fluid, p_B is the backpressure which represents the pressure at the outlet of

the microsystem and p_I is the pressure at the inlet of the microsystem. In the following, the cavitation number will be applied over the whole microsystem in order to compare different microchannel geometries and due to the fact that the static pressures could not be measured inside the microsystem.

3 Results and discussion

Cavitation and velocity measurements were carried out in two microchannel geometries in order to get a better understanding of the influence of cavitation on the fluid flow in high-pressure microchannels. The microchannel geometries were chosen to show the potential of the measurement techniques. They feature particularly high velocities, high velocity gradients and are very prone to hydrodynamic cavitation. CFD simulations with a $k-\epsilon$ model of the same geometries as used in this work, but partially varying dimensions, can be found in Beinert et al. (2012) for a qualitative comparison.

3.1 Hydrodynamic cavitation

The investigated HPMS differ to conventional microsystems especially due to their high velocities, the occurrence of hydrodynamic cavitation and the partially turbulent flow with Reynolds numbers of up to 12,000 at pressure differences of up to 500 bar. Hydrodynamic cavitation describes the process of spontaneous generation and subsequent implosion of bubbles in a flowing liquid as a result of variations in the static pressure originating from hydrodynamic effects (Martynov 2005).

3.1.1 Orifice microchannel

In Fig. 4, an orifice microchannel is depicted in which an abrupt change in the cross-sectional area leads to large vapor-filled cavities at a pressure difference of 100 bar and ambient pressure at the outlet. The color dark blue represents areas with a low fluorescent signal which can be allocated to the gaseous phase. Bright blue areas represent liquid water, observable upstream of the orifice, and a white color (highest fluorescent intensity) can be found in regions where a mixture of both phases prevails. It is assumed that reflections at the interface between both phases, especially in the case of a large number of small bubbles, lead to the increased fluorescent signal.

Upstream of the orifice, liquid water can be found. At the inlet of the orifice, the water is accelerated and in consequence the static pressure decreases. Due to the harsh edges, flow separation occurs on both sides of the orifice inlet. This flow pattern is termed *vena contracta*, where the

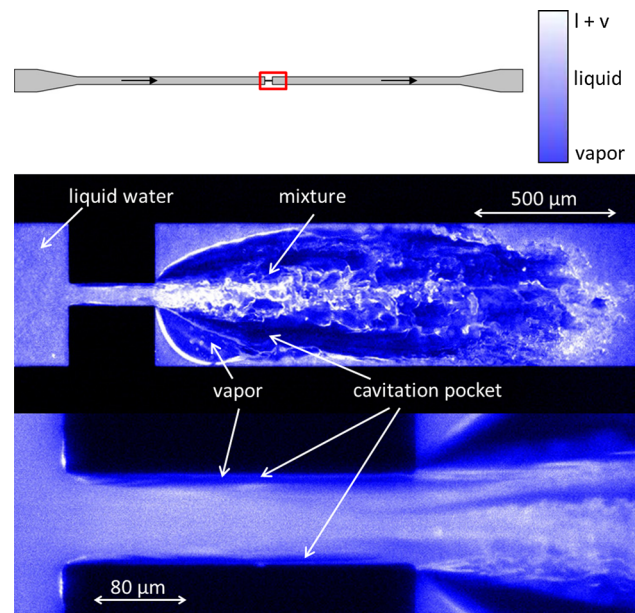


Fig. 4 Instantaneous cavitation measurements in a microchannel with an orifice [$\Delta p = 100 \text{ bar}$; $p_B = 0 \text{ bar}$ (ambient pressure)]

width of the fluid stream is the smallest and velocity is the highest. In this case, the low static pressure leads to a flow detachment from the sidewalls and vapor-filled cavities (cavitation pockets) occur and propagate downstream to the end of the orifice. This flow pattern, when the cavities reach the nozzle outlet, is termed *super-cavitation* (Sato and Saito 2001). With increasing length, the detached stream gets unstable due to turbulences and it temporarily attaches to one of the sidewalls of the orifice throat.

At the outlet of the orifice throat, the fluid leaves as a jet with a median velocity of about 90 m/s, at a pressure difference of 100 bar, into the wider channel. Due to inertial forces, the slow water close to the jet cannot follow instantaneously and the continuum of the liquid fluid breaks open. In consequence, large vapor-filled cavitation pockets occur on both sides of the jet. It is possible that moving vapor bubbles from inside the orifice contribute to the initial generation of the large cavities. Once generated, the large cavities stay relatively constant in size and shape at a constant pressure difference. Due to the large vapor-filled cavities, the jet enters into a vapor-filled wider channel. This kind of jet, entering into a wider channel filled with a gaseous phase instead of a liquid phase, will be named “free jet” in the following. After leaving the orifice, the free jet expands and breaks up into large liquid ligaments. This is called “primary breakup” which mainly results from hydrodynamic cavitation in the orifice and turbulent oscillations in the liquid (Arai et al. 1985). The “secondary breakup” leads to a further breakup of the ligaments into drops due to the surrounding vapor

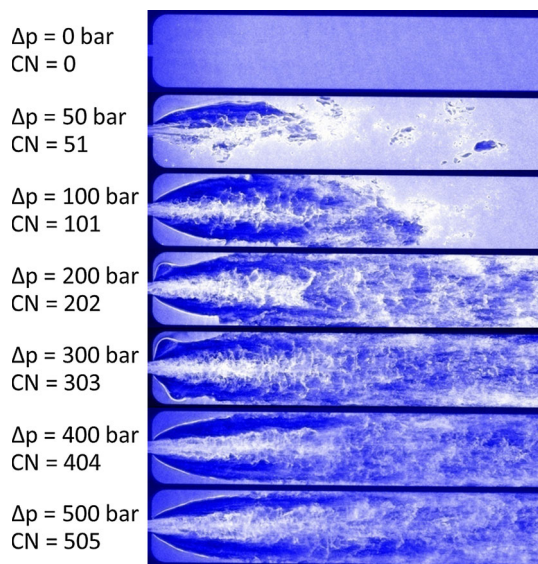


Fig. 5 Instantaneous cavitation downstream of the orifice at increasing pressure difference and ambient pressure at the outlet of the microsystem ($p_B = 0 \text{ bar}$)

(Martynov 2005). Downstream of the orifice, on the side-walls and in the corners of the wider channel, liquid water prevails which is continuously dragged along at the edges of the orifice outlet (see Fig. 4). The cavities collapse downstream of the orifice where the static pressure increases above the vapor pressure.

In Fig. 5, the development of the cavitation downstream of the orifice outlet at increasing pressure differences is depicted. With increasing pressure difference, the cavitation propagates downstream and the breakup of the jet into drops takes place earlier. At a pressure difference of 50 bar and a cavitation number of 51, only one vapor pocket is fully developed. Thus, the jet is redirected to the opposite side of the vapor pocket. Additionally, downstream traveling cavities can be observed. Probably, the missing large cavity pocket is continuously dragged along with the flow what results in the large traveling cavities which do not occur at higher pressure differences. At a pressure difference of 200 bar, only ligaments prevail in the visible channel area, whereas at a pressure difference of 400 bar and above an earlier transition to drops appears.

The cavitation pattern at a constant pressure difference of 300 bar and increasing backpressure downstream of the orifice is depicted in Fig. 6. With increasing backpressure, the area of cavitation collapse moves upstream until a cavitation number between 15.7 and 14.3 is reached and one of the two cavitation pockets collapses. There are two possible explanations for the asymmetric emergence (see Fig. 5) and disappearance (see Fig. 6) of the cavitation pockets. One reason could be the asymmetric behavior of the jet in a non-cavitating flow which will be shown in

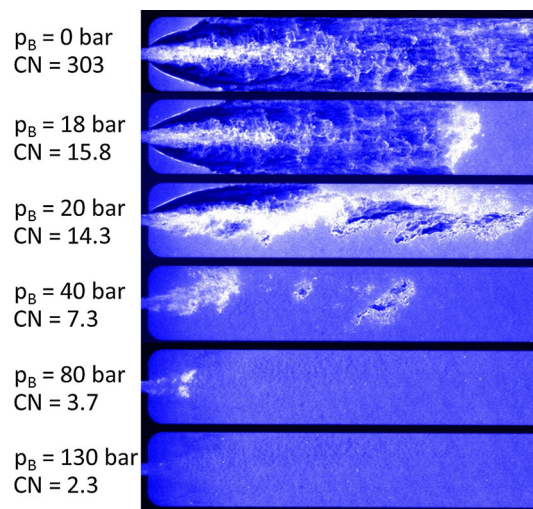
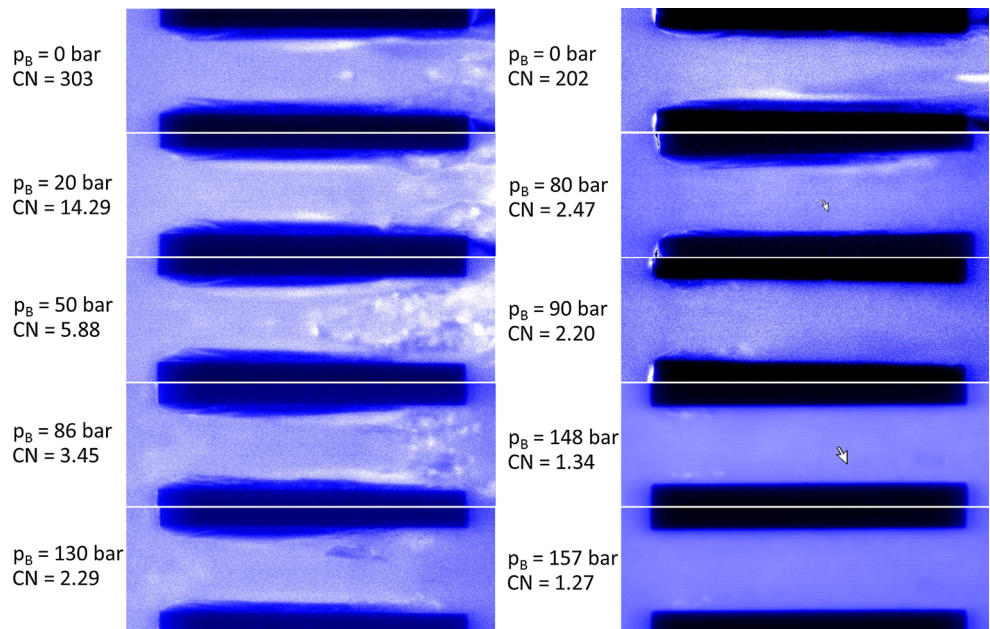


Fig. 6 Instantaneous cavitation pattern downstream of the orifice at a constant pressure difference of 300 bar and increasing backpressure

Chapter 2.3. Furthermore, small inaccuracies or deposits could lead to this asymmetric behavior. It is not a temporary phenomenon which switches from one side to the other but rather a relatively stable state at the respective pressure drop and backpressure. As already mentioned above, the absence of one cavitation pocket leads to large traveling cavities. With further increased backpressure, the second cavitation pocket collapses and a large amount of small cavitation bubbles (cavitation clouds) prevail in the areas with highest shear forces which are in between the jet and the slow water in the wider channel. A further decreasing cavitation number leads to a decrease in the amount of cavitation bubbles downstream of the orifice. At a cavitation number of 2.3, still small cavitation clouds appear occasionally. Higher backpressures could not be applied due to the fact that the application of a backpressure reduces the maximum pressure stability of the orifice microsystem from 500 to 430 bar ($\Delta p + p_B$) in this case.

The images shown in Fig. 7 with pressure differences of 300 bar (left) and 200 bar (right) with increasing backpressure are instantaneous recordings of a fluctuating cavitation pattern. The following conclusions are based on the review of at least 100 instantaneous images for each parameter variation and each magnification: At a pressure difference of 300 bar and a backpressure of 0 bar, supercavitation prevails only temporarily in the orifice. When the cavitation propagates to the outlet of the orifice throat, the cavitation pockets in the orifice throat and the cavitation pockets downstream of the orifice get connected and pressure equalization takes place. Although both cavitation pockets should exhibit the saturated vapor pressure of water, it seems to have a destabilizing effect on the cavitation pocket in the orifice. In consequence, the water stream attaches to the wall at the last quarter of the orifice

Fig. 7 Instantaneous cavitation in the orifice throat at a constant pressure difference of 300 bar (left) and 200 bar (right) and increasing backpressure



throat and the cavitation flow switches from super-cavitation to transition-cavitation (Sato and Saito 2001). Additionally, cavitation bubbles occur within the liquid water stream which can be seen especially in the image at a cavitation number of 5.88 in Fig. 7. The whole cavitation pattern in the orifice is very instable.

With increasing backpressure, super-cavitation is eliminated and transition-cavitation prevails in the orifice throat. When super-cavitation is eliminated entirely, the mean length of the vapor pockets stays almost constant but underlies minor fluctuations which can be seen especially in the cavitation images at a pressure difference of 300 bar. At a pressure difference of 200 bar and a backpressure between 80 and 90 bar, the cavitation pockets are relatively abruptly restricted to the vena contracta (see Fig. 7 right). At a pressure difference of 300 bar, the maximum backpressure of 130 bar was not sufficient to show this effect. With further increasing backpressure, the vapor pockets disappear and only clouds of cavitation bubbles appear in the vena contracta (white areas). At a backpressure of 157 bar, the cavitation clouds appear only occasionally. At a backpressure of about 160 bar, which corresponds to a cavitation number of 1.24 all visible cavitation is eliminated at a pressure difference of 200 bar ($p_I = 360$ bar, $p_B = 160$ bar).

At a constant pressure difference, the volume flow increases linearly with increasing backpressure until a critical backpressure is reached (see Fig. 8). Above this critical backpressure, the volume flow is independent of the backpressure. For a pressure difference of 200 bar, the critical backpressure has a value of about 90 bar, and hence, it is consistent with the backpressure which is

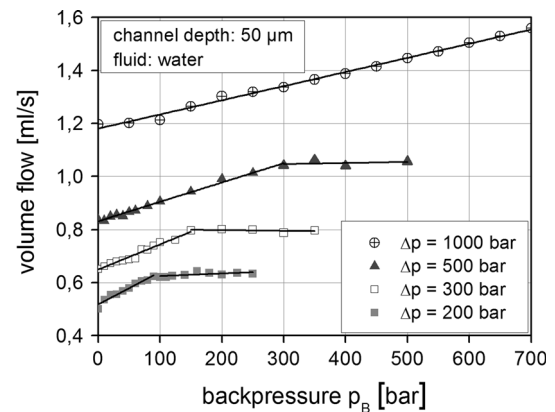


Fig. 8 Volume flow at a constant pressure difference of 200, 300, 500 and 1,000 bar and varying backpressures

required to restrict cavitation to flow detachment in the vena contracta (see Fig. 7 right). Hence, if the cavitation pockets in the orifice throat are restricted to the area of flow detachment in the vena contracta, the remaining cavitation does no longer influence the volume flow. With increasing pressure difference, the ratio between the critical backpressure, at which the volume flow gets constant, and the pressure difference ($p_{B, \text{crit.}}/\Delta p$) increases.

3.1.2 T-microchannel

In the T-microchannel, the flow is separated at first and merged downstream (see Fig. 9). At the conjunction the flow detaches, due to the harsh edges and the high velocity of the flow, from the sidewalls and cavitation pockets occur next to the out streaming jets. The two jets merge in the

center of the wider channel and are deflected in a 90° angle. The merged liquid water stream passes through a primary and secondary breakup like in the orifice microchannel. In contrast to the orifice geometry, the collapse of the cavitation is less focused but extends along a wider range beginning in the middle of the primary breakup. The vapor condenses on the sidewalls of the wider channel where velocity is lower and static pressure increases.

With increasing backpressure at a constant pressure difference of 300 bar, again at first the area of collapse moves upstream like in the orifice geometry (see Fig. 10). With further increasing backpressure, one of the cavitation pockets collapses. Small asymmetries, resulting from the fabrication process, lead to a disparity of the volume flows in the two channel arms of the T-microchannel. In consequence, the cavitation pocket next to the channel arm with the lower volume flow collapses first. At a cavitation number of 5.9, no more cavitation is visible.

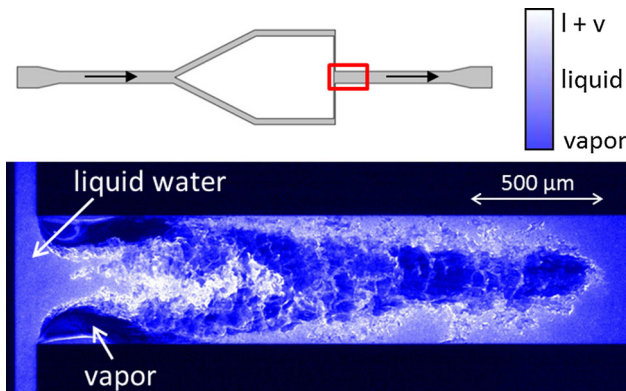
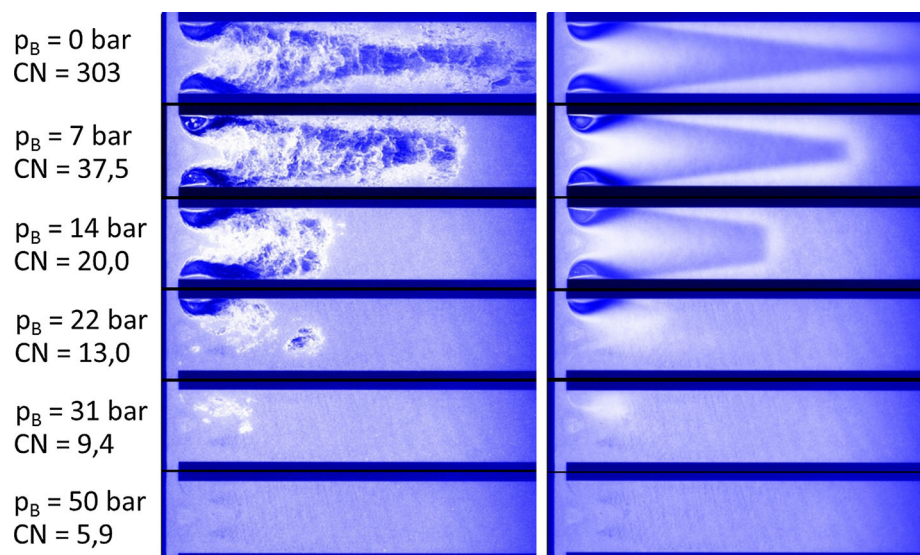


Fig. 9 Instantaneous cavitation pattern in a T-microchannel at the conjunction at a pressure difference of 200 bar and ambient pressure at the outlet of the microsystem ($p_B = 0$ bar)

Fig. 10 Cavitation pattern at the junction in the T-microchannel at a constant pressure difference of 300 bar and increasing backpressure; *left* instantaneous; *right* averaged



3.2 Velocity measurement

In order to carry out velocity measurements with μ PIV, cavitation has to be eliminated in most instances. Otherwise, the tracer particles are invisible due to the reflections at the cavitation bubbles.

In Fig. 11a, the velocity measurement in the middle height of the orifice microchannel (middle height = 26 μ m) at a pressure difference of 300 bar and a backpressure of 120 bar is depicted. Upstream of the orifice the flow is laminar with a velocity of about 30 m/s. At the inlet of the orifice, the flow is accelerated within a few micrometers to about 190 m/s which leads to a Reynolds Number of about 11,500. Downstream of the orifice, the jet is decelerated and redirected to one sidewall. The side to which the jet is redirected is random although little asymmetries of the microchannel can lead to a preferred side. Usually, the jet stays at one side during an experiment and only once a changeover could be observed. On the opposite side of the redirected jet, a backflow occurs due to the suction of the incoming jet.

The velocity vector field of the T-microchannel at a pressure difference of 500 bar and a backpressure of 60 bar is depicted in Fig. 11b. The cavitation is eliminated by the backpressure, and in consequence, a backflow occurs on one side of the channel and the merged jet is redirected to the opposite side. The side to which the jet is redirected is determined by the height of the volume flows in the two channel arms. The two jets do not converge frontally but are redirected and converge tangentially.

Velocities in the narrowest part of the microchannels reach about 190 m/s in the orifice microchannel ($\Delta p = 300$ bar) and about 185 m/s in the T-microchannel ($\Delta p = 500$ bar). Comparing these results with the median velocities calculated from mass flow measurements in

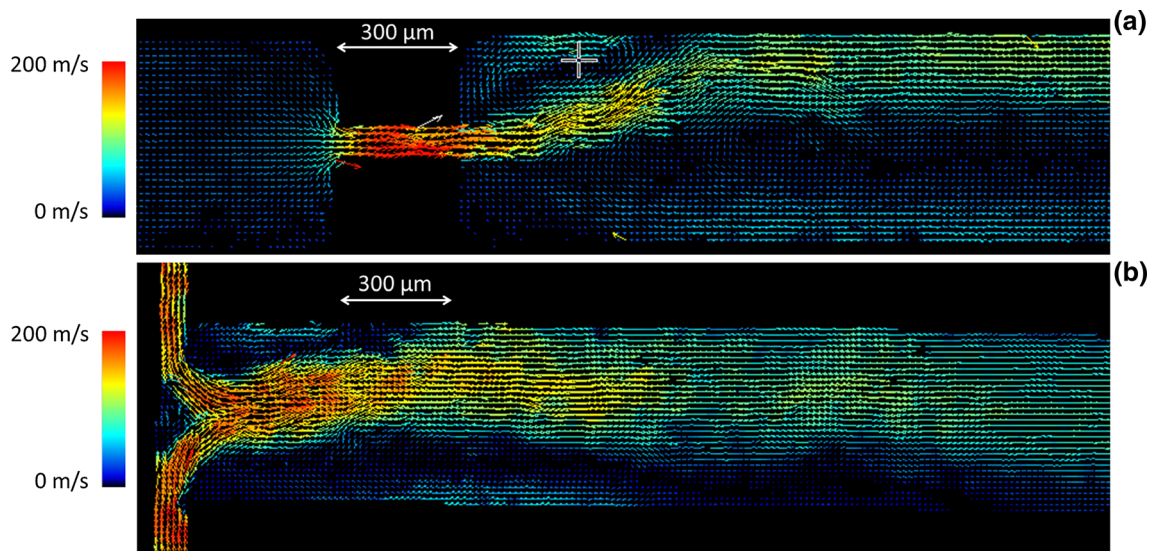


Fig. 11 Instantaneous velocity measurements in the orifice microchannel with μ PIV at a pressure difference of 300 bar and a backpressure of 120 bar at the middle channel height of 26 μ m (a);

velocity measurements in T-microchannel with μ PIV at a pressure difference of 500 bar and a backpressure of 60 bar at the middle channel height of 25.5 μ m (b)

Table 1 Flow parameters in the narrowest microchannel of the respective geometry calculated from mass flow measurements

Geometry	Δp [bar]	p_c [bar]	Flow rate [mL/s]	Mean velocity [m/s]	Reynolds number [-]	Hydraulic diameter [μ m]
Orifice	300	120	0.7636	187.2	11,646	62.29
T-geometry	500	60	1.6260	190.7	12,122	63.64

Table 1, it can be stated that they coincide very well. But, regarding the accuracy of the velocity measurements in HPMS in general, some restrictions have to be considered. At such high fluid velocities, in combination with the magnification, these measurements are at the limit of commercially available cameras suitable for this application regarding the interframing time. Hence, in measurements with higher velocities than about 200 m/s, the particle displacement increases far above the optimum and the accuracy of the measurements decreases. Additionally, μ PIV inherently is less accurate in areas with high velocity gradients which are very distinct in the HPMS. The interframing time was adjusted to the highest velocities. In consequence, the measuring error at low velocities increases.

3.3 Comparison of orifice- and T-microchannel

The orifice microchannel is more prone to cavitation than the T-microchannel. At a constant pressure difference of 300 bar, a cavitation number of 5.9 is sufficient to eliminate the visible cavitation in the T-microchannel, whereas a cavitation number of 1.24 has to be reached in the orifice microchannel. Beside the higher velocities in the orifice microsystem, especially the channel geometry leads to different susceptibilities to cavitation. The dependency of the volume flow on the backpressure could only be found

in the orifice geometry. The T-microsystem delivered constant volume flows at increasing backpressures.

Both geometries are suitable for dispersion and emulsification processes, which was shown in previous publications (Gothsch et al. 2011; Finke et al. 2012). Furthermore, due to the high turbulence which enables high mixing rates, both geometries could be applied in precipitation processes and other processes in which high and adjustable mixing rates are required (Zhdanov and Chorny 2011; Chorny and Zhdanov 2012). Regarding the susceptibility to cavitation, which is a source of abrasion in microchannels, the T-geometry has advantages compared to the orifice geometry.

4 Conclusion

High-pressure microfluidic systems exhibit special features like high volume flows, turbulent flow, which can be utilized for high-speed mixing processes and high shear forces, which enable, for example, deagglomeration or emulsification processes. A combination of high-pressure processes with conventional low-pressure processes is feasible on only one microsystem by parallelizing microchannels. In consequence, HPMS extend the possibilities of microprocess engineering.

In contrast to the laminar flow in low-pressure microsystems, the prediction of the flow in HPMS by means of CFD simulations is much more complex and less accurate. Main reasons are the simultaneous presence of turbulent flow and cavitating (two-phase) flow. Therefore, especially in the development of complex HPMS flow and process characterization is a basic requirement. With the presented techniques, beginning with the fabrication process over the pressure stabilization up to the high-speed flow characterization, a complete concept of a HPMS for research applications and a tool for the development of high-pressure processes in microsystems is introduced.

Acknowledgments The authors gratefully acknowledge the DFG for financial support within the DFG research group 856 “Microsystems for particulate life-science-products” (mikroPART) and the mikroPART group. One of the authors (S. Bü.) gratefully acknowledges the financial support of the Volkswagen Foundation.

References

- Arai M, Shimizu M, Hiroyasu H (1985) Breakup length and spray angle of high speed jet. In: 3rd International conference on liquid atomization and spray systems (ICLASS), London
- Beinert S, Gothsch T, Kwade A (2012) Numerical evaluation of flow fields and stresses acting on agglomerates dispersed in high-pressure microsystems. *Chem Eng Technol* 35(11):1922–1930
- Büttgenbach S, Balck A, Demming S, Lesche C, Michalzik M, Al-Halhouli AT (2009) Development of on chip devices for life science applications. *Int J Eng* 3:148–158
- Capretto L, Carugo D, Mazzitelli S, Nastruzzi C, Zhang X (2013) Microfluidic and lab-on-a-chip preparation routes for organic nanoparticles and vesicular systems for nanomedicine applications. *Adv Drug Deliv Rev* 65(11–12):1496–1532. doi:10.1016/j.addr.2013.08.002
- Chorny A, Zhdanov V (2012) Turbulent mixing and fast chemical reaction in the confined jet flow at large Schmidt number. *Chem Eng Sci* 68(1):541–554. doi:10.1016/j.ces.2011.10.015
- Finke JH, Schur J, Richter C, Gothsch T, Kwade A, Büttgenbach S, Müller-Goymann CC (2012) The influence of customized geometries and process parameters on nanoemulsion and solid lipid nanoparticle production in microsystems. *Chem Eng J* 209:126–137. doi:10.1016/j.cej.2012.07.115
- Gothsch T, Finke JH, Beinert S, Lesche C, Schur J, Büttgenbach S, Müller-Goymann C, Kwade A (2011) Effect of microchannel geometry on high-pressure dispersion and emulsification. *Chem Eng Technol* 34(3):335–343
- Gravesen P, Branbjerg J, Jensen OS (1993) Microfluidics-a review. *J Micromech Microeng* 3(4):168
- Håkansson A, Fuchs L, Innings F, Revstedt J, Bergenstahl B, Trägårdh C (2010) Visual observations and acoustic measurements of cavitation in an experimental model of a high-pressure homogenizer. *J Food Eng* 100(3):504–513. doi:10.1016/j.jfoodeng.2010.04.038
- Lee C-Y, Chang C-L, Wang Y-N, Fu L-M (2011) Microfluidic mixing: a review. *Int J Mol Sci* 12(5):3263–3287
- Lesche C, Gothsch T, Kwade A, Büttgenbach S (2011) Development of a dispersion micro-element for pharmaceutical screening applications: material and fabrication. In: Proceedings of MST Kongress 2011, Darmstadt, Germany, pp 642–645
- Li H, Olsen MG (2006a) MicroPIV measurements of turbulent flow in square microchannels with hydraulic diameters from 200 μm to 640 μm . *Int J Heat Fluid Flow* 27(1):123–134
- Li H, Olsen MG (2006b) Examination of large-scale structures in turbulent microchannel flow. *Exp Fluids* 40:733–743. doi:10.1007/s00348-006-0110-4
- Li H, Ewoldt R, Olsen MG (2005) Turbulent and transitional velocity measurements in a rectangular microchannel using microscopic particle image velocimetry. *Exp Thermal Fluid Sci* 29(4):435–446
- Martynov S (2005) Numerical simulation of the cavitation process in diesel fuel injectors. University of Brighton, Brighton
- Mishra C, Peles Y (2005) Flow visualization of cavitating flows through a rectangular slot micro-orifice ingrained in a microchannel. *Phys Fluids* 17(11):1–14
- Phipps LW (1974) Cavitation and separated flow in a simple homogenizing valve and their influence on the break-up of fat globules in milk. *J Dairy Res* 41(01):1–8. doi:10.1017/S0022029900014849
- Richter C, Stegemann D, Vierheller A, Gothsch T, Finke JH, Kwade A, Müller-Goymann CC, Dietzel A, Büttgenbach S (2013) Innovative process chain for the development of wear resistant 3D metal microsystems. *Microelectron Eng* 110(0):392–397. doi:10.1016/j.mee.2013.02.078
- Salvador FJ, Martínez-López J, Caballer M, De Alfonso C (2013) Study of the influence of the needle lift on the internal flow and cavitation phenomenon in diesel injector nozzles by CFD using RANS methods. *Energy Convers Manag* 66(0):246–256. doi:10.1016/j.enconman.2012.10.011
- Sato K, Saito Y (2001) Unstable cavitation behavior in a circular-cylindrical orifice flow. In: Fourth international symposium on cavitation: CAV 2001, California Institute of Technology, Pasadena, CA
- Sou A, Hosokawa S, Tomiyama A (2007) Effects of cavitation in a nozzle on liquid jet atomization. *Int J Heat Mass Transf* 50(17–18):3575–3582. doi:10.1016/j.ijheatmasstransfer.2006.12.033
- Suh HK, Lee CS (2008) Effect of cavitation in nozzle orifice on the diesel fuel atomization characteristics. *Int J Heat Fluid Flow* 29(4):1001–1009. doi:10.1016/j.ijheatfluidflow.2008.03.014
- Zhdanov V, Chorny A (2011) Development of macro- and micro-mixing in confined flows of reactive fluids. *Int J Heat Mass Transf* 54(15–16):3245–3255. doi:10.1016/j.ijheatmasstransfer.2011.04.006